Journal of Energy Chemistry 45 (2020) 91–97

Contents lists available at ScienceDirect

Journal of Energy Chemistry

journal homepage: www.elsevier.com/locate/jechem

http://www.journals.elsevier.com/journal-of-energy-chemistry/

3D-printing of integrated spheres as a superior support of phosphotungstic acid for deep oxidative desulfurization of fuel

Jie Zhu[a], Peiwen Wu[a], Linlin Chen[a], Jing He[a], Yingcheng Wu[b], Chao Wang[c], Yanhong Chao[a], Linjie Lu[a], Minqiang He[a], Wenshuai Zhu[a,*], Huaming Li[a]

[a] School of Chemistry and Chemical Engineering, Institute for Energy Research, Jiangsu University, Zhenjiang 212013, Jiangsu, China
[b] Zhenjiang Sandi New Materials Co., Ltd., Zhenjiang 212013, Jiangsu, China
[c] School of the Environment and Safety Engineering, Institute of Environmental Health and Ecological Security, Jiangsu University, Zhenjiang 212013, Jiangsu, China

ARTICLE INFO

Article history:
Received 19 July 2019
Revised 27 September 2019
Accepted 1 October 2019
Available online 14 October 2019

Keywords:
3D printing
Integrated spheres
Supported catalyst
Oxidative desulfurization

ABSTRACT

Construction of catalysts with integral structure for oxidative reaction process is an essential promotion to catalysts in industrial application. In this work, a 3D printing method was employed to prepare 3D printed spheres (3D-PSs), followed by carbonization to form 3D carbon spheres (3D-CSs). Then, a 3D-CSs supported phosphotungstic acid (HPW/3D-CSs) was prepared for deep oxidative desulfurization. Compared with traditional powder catalysts, the as-prepared catalyst is easy to be operated and separated from oil products. The supported catalyst possesses excellent catalytic performance and the removal of DBT, 4-MDBT and 4, 6-DMDBT in fuel oil, reaching ~100% of sulfur removal. The effects of various experimental parameters on desulfurization efficiency were considered to optimize reaction conditions. Moreover, the catalyst shows excellent thermal and chemical stability, with no obvious decrease in desulfurization activity after 5 cycles. GC–MS analysis indicates DBT sulfone was the solely oxidized product of DBT.

1. Introduction

The SO_x emission from combustion of sulfur compounds in fuel oil has become a main source of environmental pollutions [1–5]. Thus, in the past few decades, because of the increasingly serious environmental issues, regulations on sulfur compounds have turned to be more and more stringent [6]. Currently, the sulfur content in transport oil is limited to be no more than 10 ppm [7,8], and the value in fuel cell is more stringent, which is required to be lower than 60 ppb [9]. Industrially, the sulfur compounds in fuel oils are generally removed by hydrodesulfurization (HDS), which is realized at high reaction temperature and operating pressure [10], and hydrogen is always required in HDS process [11]. All these reaction conditions make HDS a relatively high-cost technology [12]. Most importantly, because of the poor activity to aromatic sulfur compounds [13], realization of deep desulfurization via HDS process requests harsher reaction conditions [14]. Thus, numerous desulfurization technologies, such as extractive desulfurization (EDS) [15–18], adsorptive desulfurization (ADS) [19–21], oxidative desulfurization (ODS) [22–26], have been developed. Among all those newly-emerged approaches, ODS has been regarded as a promising one [27], because of the high activity to aromatic sulfur compounds under mild conditions.

To achieve superior ODS efficiency, an inevitable topic is seeking for a highly-active catalyst [28]. Up to date, numerous catalysts have been explored, such as metal oxides [14,29], heteropolyacids [30], task-specific ionic liquids [31–33], two-dimensional nanocatalysts [34–36]. Among them, heteropolyacids have been widely employed for ODS. Because of the variable valences of catalytic active sites in heteroloyacids, a boosted heteropolyacids is always expected in ODS [37]. However, the most significant disadvantage is that the heteropolyacids catalysts are of low specific surface areas, leading to the poor exposure of catalytically active sites. Thus, heteropolyacids are generally loaded onto supports to fabricate supported catalysts. The supported catalysts not only can maximize the utilization of catalytic active sites, but also can reduce the consumption of heteropolyacids without significant decrease in catalytic performance. So far, numerous materials, such as porous silica [38], metal oxides [39–41], graphene [42], boron nitride [43–45], have been widely employed in preparation of supported catalysts. By this approach, satisfying oxidative desulfurization

* Corresponding author.
E-mail address: zhuws@ujs.edu.cn (W. Zhu).

https://doi.org/10.1016/j.jechem.2019.10.001

performance has paid back. However, since all these catalysts are presented in powder forms, making them difficult to be separated from fuel oil [46]. Moreover, molding of the catalysts to form integral catalysts is seriously limited by the technology and costs [47]. Both the disadvantages make the developed catalysts difficult to be utilized industrially.

More recently, three dimensional (3D) printing technology, a newly-emerged additive manufacturing strategy [48,49], has gained increasing attention worldwide [50,51]. 3D printing technology can be widely used in the integral catalyst, mixer and reactor [52]. With the continuous development of 3D printing technology, printing accuracy and material performance have been significantly improved [53]. Therefore, it provides a great advantage for the research of catalytic and adsorptive materials. By using 3D printing technology, formulated catalysts with different structures, especially complex ones, can be easily realized by fewer steps [54]. Theoretically, almost all designed catalyst structures can be brought to practical ones flexibly. Additionally, by employing 3D printing method, the utilization rate of raw materials can be promoted remarkably [55]. Most importantly, the 3D printing can generate integral catalysts directly [56,57], making the separation of catalysts and reaction system more easily [49]. Thusly, construction of catalysts by 3D-printing technology can overcome the disadvantages of traditional powder catalysts, which makes the technology to be a potential technology to impel traditional powder oxidative desulfurization catalysts to industrial application.

In this contribution, we employed a photocuring 3D-printing technology to prepare oxidative desulfurization catalysts. Initially, the structure of the sphere was designed by a 3Ds Max with a diameter of 1 cm. Afterwards, a photocuring 3D-printer with photocurable resins as raw materials was used to realize the design, and 3D printing spheres (3D-PSs) were obtained. The 3D-PSs were carbonized to form 3D carbon spheres (3D-CSs), and further employed as the support to anchor phosphotungstic acid (HPW). The structure of the prepared catalyst (HPW/3D-CSs) was determined by a series of characterization. Moreover, an excellent catalytic performance of HPW/3D-CSs, that a 100% of sulfur removal, was obtained in catalytic oxidative desulfurization. Most importantly, the catalyst can be recycled by a simple filtration without centrifugation or other separation methods. The catalyst can be recycled for 5 times without significantly reducing catalytic activity. This work would provide a novel strategy to design highly-active and easily-reusable catalysts for oxidative desulfurization.

2. Experimental

2.1. Materials

$H_3PW_{12}O_{40}$ (AR grade), ethanol (AR grade) and hydrogen peroxide (H_2O_2, 30 wt%) were purchased from Sinopharm Chemical Reagent Co., Ltd. Glacial acetic acid (99%) was purchased from Aladdin. Dibenzothiophene (DBT, 98%), 4-methyldibenzothiophene (4-MBDT, 96%) and 4, 6-Dimethyldibenzothiophene (4, 6-DMDBT, 97%) were purchased from Sigma-Aldrich. The DLP photo-cured 3D printer (MoonRay-S) and 3D printing resin (SP-RH1001) were purchased from Zhejiang Xunshi Technology Co., Ltd.

2.2. Preparation of the catalysts

Three-dimensional spheres with diameters of 1 cm were designed by a 3Ds Max software. Then, the designed three-dimensional model was printed out by a photo-cured 3D printer with photo-cured resin as the raw materials [58]. The 3D printing spheres (3D-PSs) were heated to 900 °C with a ramping rate of 0.5 °C/min in N_2 atmosphere, and was kept at 900 °C for another 120 min to ensure that the 3D printing spheres were completely carbonized. Afterward, the tube furnace was naturally cooled to room temperature and the carbonized 3D carbon spheres (3D-CSs) was obtained. Then, a certain amount of phosphotungstic acid (HPW) was dissolved in ethanol, and CSs were added into the reaction bottle and kept magnetically stirring for 24 h. After impregnation, the ethanol solution was removed by evaporating the solution thermally, and the obtained catalyst (HPW/CSs) was dried in vacuum oven overnight. The catalysts with different HPW loading amount was denoted as HPW/CSs-1, HPW/CSs-4, HPW/CSs-7, and HPW/CSs-10, respectively.

2.3. Characterization of the catalysts

Scanning electron microscopy (SEM) was used to analyze the surface morphology of the catalyst at 2–15 keV acceleration voltage. Elemental analysis was performed by energy dispersive X-ray spectroscopy (EDS). The powder X-ray diffraction (XRD) measurements was launched on a Bruker D8 diffractometer with high-intensity Cu K_α radiation ($\lambda = 1.54$ Å), ranging from 5° to 80° with the scanning speed of 5°/min. Fourier transform infrared spectroscopy (FT-IR) was obtained by using KBr pellets on Fourier transform infrared spectrometer (Nicolet Nexus 470). The gas chromatography-mass spectrometry (GC–MS) detection was carried out on Agilent 7890/5975C-GC/MSD (temperature program: 100–230 °C rising at 15 °C/min, 230–250 °C rising at 10 °C/min, HP-5 MS column) to determine the oxidized product after 30 min of the reaction.

2.4. Procedure of oxidative desulfurization

Different model oils with 200 ppm of S content were prepared by dissolving DBT, 4-MDBT and 4, 6-DMDBT in dodecane and adding hexadecane as internal standard. In this oxidative desulfurization process, a mixture including a certain amount of catalyst, 5 mL model oil with 200 ppm of S content, 1 mL glacial acetic acid (HAc) and the required amount of H_2O_2 in a double-necked flask was stirred magnetically at 70 °C. In the cyclic experiment, the catalysts of the previous reaction were filtered directly and reacted under the same conditions.

3. Results and discussion

3.1. Characterization of the catalysts

To visually exhibit the preparation process of the catalysts, the photographs of preparation process was recorded in Fig. 1. Initially, the structure of the integrated 3D-PSs was designed by 3Ds Max. As shown in Fig. 1(a), the designed 3D-PSs are porous hollow spheres with a diameter of 1 cm, and the pores are connected to each other, which is beneficial to the transfer during the catalytic process. Afterwards, the designed 3D-PSs were obtained by a light-curing 3D printer with light-curable resin as the raw material. The optical photograph of the printed 3D-PSs in Fig. 1(b) shows that the structure of the printed 3D-PSs is similar to that of the designed one, indicating that the 3D printing strategy can effectively realize the design of the catalyst's structure. Subsequently, the 3D-PSs were carbonized at high temperature in N_2 atmosphere. As shown in Fig. 1(c), the diameter of the 3D-CSs after carbonization at 900 °C was measured to be about 0.5 cm, which is caused by the shrink of 3D-PDs during the carbonization process. The color of the 3D-CSs was silver gray with metallic luster. After carbonization, the sphere structure and pore channels still remained, and no collapse was detected. The result shows that the carbonization process also does not destroy the structure of 3D printed sphere. As shown in Fig. 1(d), after loading HPW, the morphology of HPW/3D-

Fig. 1. (a) Designed structure of 3D-PSs by 3Ds max; optical photos of the samples: (b) 3D-PSs; (c) 3D-CSs; (d) HPW/3D-CSs.

CSs is similar to that of 3D-CSs, illustrating that the impregnation process did not change the structure of 3D-CSs significantly.

The mechanical strength of HPW/3D-CSs is of great significance for the use of HPW/3D-CSs. The mechanical strength of HPW/3D-CSs was observed by testing its crush strength. As shown in Fig. S1(a), HPW/3D-CSs were first placed on the test platform. Then the platen slowly dropped (Fig. S1b) until it was firmly attached to the surface of HPW/3D-CSs (Fig. S1c). Finally, HPW/3D-CSs ruptured instantaneously (Fig. S1d) when the impact energy reached a certain level. The crush strength test results of HPW/3D-CSs were shown in Table S1. The crush strength of HPW/3D-CSs ranged from 110.00 MPa to 140.00 MPa, with an average value of 127.80 MPa. It is not difficult to see that the crush strength of HPW/3D-CSs is relatively high. Therefore, HPW/3D-CSs has good mechanical strength.

The surface morphology of the samples was analyzed by SEM and the chemical composition of the samples was further analyzed by EDS. Since the prepared 3D-CSs is centimeter-sized, the 3D-CSs and HPW/CSs were pulverized into small pieces for SEM and EDS analysis. As shown in the SEM image (Fig. 2(a)) that the surface of the 3D-CSs was relatively smooth, and no obvious pore was found, indicating that the pores of 3D-printed 3D-CSs is macroscopically. Fig. 2(b) and (c) shows that the surface of HPW/3D-CSs was relative smooth. Some additional bright dots were detected, which was attributed to the HPW. HPW can distribute evenly on the surface of 3D-CSs. The EDS analysis of HPW/3D-CSs was further carried out in Fig. 2(d), showing that C, O, and W elements existed in the sample. The results indicated that the active component HPW was successfully loaded onto the 3D-CSs.

Furthermore, FT-IR spectrum was performed to determine the composition of the prepared HPW/3D-CSs. As shown in Fig. 3(a), four strong characteristic peaks were found at 1076 cm^{-1} (P–O), 978 cm^{-1} (W==O), 890 cm^{-1} (W–O_b–W) and 800 cm^{-1} (W–O_c–W) [59], which were assigned to typical Keggin structure of HPW [60]. The FT-IR spectrum of 3D-CSs exhibits that no evident peak was detected, indicating that there are almost no functional groups on the surface of the 3D-CSs. The FT-IR spectrum of 3D-CSs is similar to that of pure carbon materials [61], illustrating that the 3D-PSs have been totally carbonized to 3D-CSs. Compared with FT-IR spectra of 3D-CSs and HPW, the characteristic peaks for Keggin structure of HPW were clearly explored. The result indicates that HPW has been loaded onto 3D-CSs.

XRD patterns were shown in Fig. 3(b) to characterize the composition of the prepared catalysts. Fig. 3(b) shows the XRD pattern of HPW that characteristic diffraction peaks for HPW were clearly detected at $2\theta = 10.3°$, 20.7°, 23.1°, 25.4° and 29.5° [62]. In addition, the XRD pattern for 3D-CSs was performed, and only two characteristic peaks at $2\theta = 24.9°$ and 43.8° were detected, respectively assigning to the (002) lattice and (100) lattice of carbon materials [63]. No additional peak was found, demonstrating that the 3D-PSs have been totally carbonized to 3D-CSs. Moreover, it can be seen from the XRD pattern of HPW/3D-CSs that both the characteristic peaks for HPW and 3D-CSs were clearly seen, indicating that the HPW has been loaded onto 3D-CSs, and the structures were not destroyed.

3.2. Optimization of oxidative desulfurization parameters

In order to achieve better desulfurization performance, we investigated the effects of reaction temperatures, HPW loading amount, molar ratios of oxidant to sulfur-containing substrates, and catalyst dosages to optimize the reaction parameters.

As shown in Fig. 4(a), we investigated the effect of reaction temperatures on the desulfurization activity [64]. As shown in the result that the desulfurization performance of the catalyst at different temperatures follows the order of 70 °C > 80 °C > 60 °C > 50 °C in turn. From the comparative experiments, the most optimized reaction temperature was 70 °C, and the removal of DBT reached 100% after 2 h of reaction. The reason may be concluded as following: at lower reaction temperature, the oxidant cannot be effectively activated. However, when the reaction temperature further raised to 80 °C, the self-decomposition of H_2O_2 turns to be more serious, leading to a lower desulfurization activity.

The effect of HPW loading on the oxidative desulfurization activity of the catalyst was shown in Fig. 4(b). It can be clearly seen from the figure that the desulfurization performance of the catalysts follows the following orders: HPW/3D-CSs-7 > HPW/3D-CSs-10 > HPW/3D-CSs-4 > HPW/3D-CSs-1. The results show that the desulfurization effect of the catalyst is better when the loading amount is 7%. Compared with low loading, more active sites could be achieved when the loading amount was 7%. When the HPW loading further increased to higher than 7%, the desulfurization rate could still reach 100%, but the reaction rate of desulfurization become slower. This might be assigned to the agglomeration of active components on the surface of the 3D-CSs after carbonization, resulting in a slower reaction rate.

The amount of oxidant is an important factor in the oxidative desulfurization reaction [65]. As shown in Fig. 4(c), the effect of different molar ratios of oxidant to sulfur-containing substrates (O/S) on the desulfurization activity of the catalysts were investigated. The desulfurization performance increased with the increment of O/S, and the most satisfying O/S was found to be 8. Compared with the stoichiometric value, the optimal value of O/S == 8 was a little higher due to two competing reactions between the oxidation of DBT by hydrogen peroxide and the unproductive self-decomposition of hydrogen peroxide.

Fig. 4(d) displayed the effect of catalyst dosage on sulfur removal. The desulfurization efficiency was obviously related to the amount of catalyst. The efficiency of DBT removal increased with the increase of catalyst dosage, which was attributed to the increase of total active sites. When the amount of catalyst was three HPW/3D-CSs (0.12 g, ± 5%), the desulfurization rate could reach 97.1%. When the amount of the catalyst reached five HPW/3D-CSs (0.20 g, ± 5%), the reaction rate was obviously accelerated, and the desulfurization activity reached 100%. Therefore, five HPW/3D-CSs (0.20 g, ± 5%) were selected as suitable catalyst dosage.

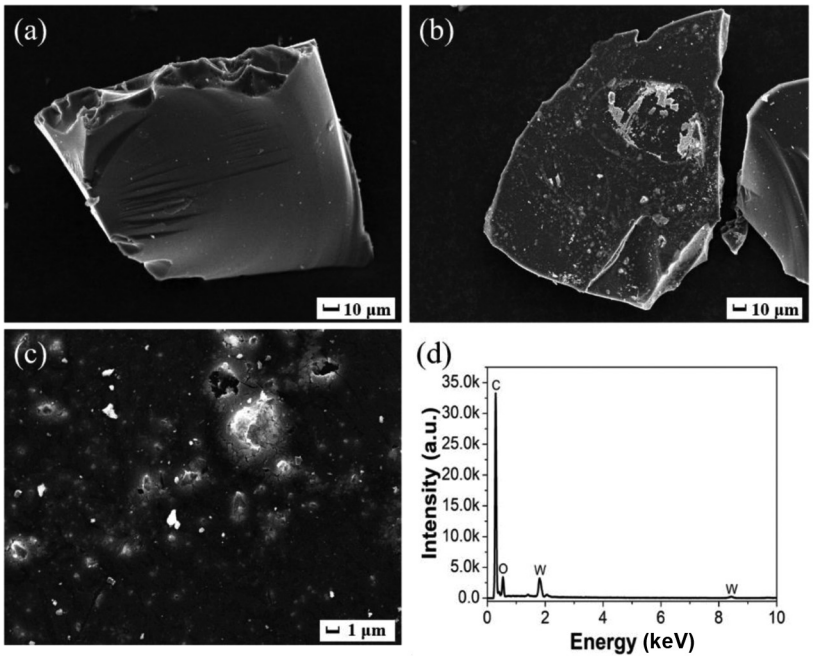

Fig. 2. SEM images of the samples: (a) 3D-CSs, (b, c) HPW/3D-CSs; and (d) EDS of HPW/3D-CSs.

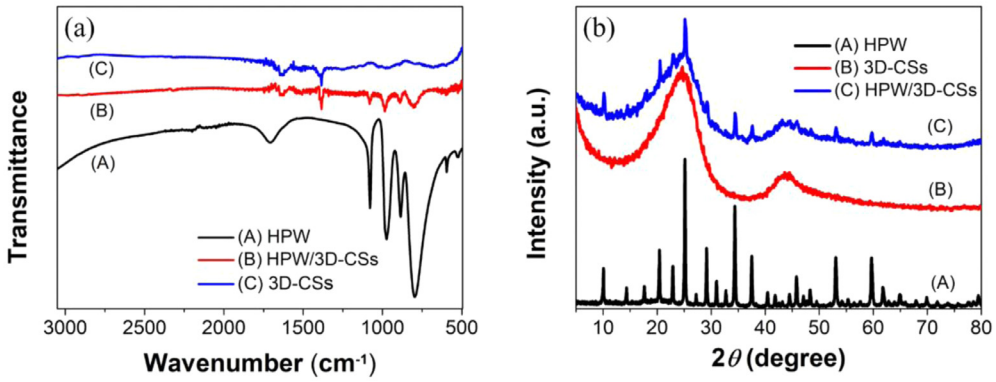

Fig. 3. (a) FT-IR spectra of (A) HPW, (B) HPW/3D-CSs, (C) 3D-CSs; (b) XRD patterns of (A) HPW, (B) 3D-CSs, (C) HPW/ 3D-CSs.

3.3. Effect of the feature of different substrates

The feature of the substrates is one of the vital factors to affect the sulfur removal in the desulfurization reaction [66]. Under the same conditions, the oxidative desulfurization performance of HPW/3D-CSs for 4-MDBT and 4, 6-DMDBT were also studied. As can be seen in Fig. 5, the catalyst possesses an excellent sulfur removal performance on DBT, 4-MDBT and 4, 6-DMDBT. After 2.5 h of reaction, the sulfur removal of all three substrates reached 100%. The reaction rate of DBT was faster than that of 4-MDBT and 4, 6-DMDBT in terms of desulfurization rate. This may be due to the differences of different electron densities on sulfur atoms and different steric hindrances of sulfur compounds [67].

3.4. Recycle of the catalyst

The recycling performance is a vital index to evaluate the performance of catalyst [68]. Compared with traditional powder catalyst, the obtained HPW/3D-CSs is a monolithic catalyst during the catalytic oxidative desulfurization process (Fig. 6), which is very beneficial to the separation of the catalyst. After the first reaction, the catalyst spheres were directly removed from the model oil by filtration, and no centrifugation or standing was required (detailed separation process see Supplementary video). The catalyst was then directly employed for the next reaction. The regenerative catalyst, fresh model oil, glacial acetic acid and hydrogen peroxide were then added to the reaction vessel for next cycle. Fig. 7 displayed the performance of the HPW/3D-CSs catalyst in removing DBT after five reuses. The results indicated that the catalyst still had good performance after five reuses. After five reuses, the sulfur removal decreased from 100% to 93.3%. It may be originated from the accumulation of that the oxidation products of DBT on the catalyst surface with the increase of cycle times. Nevertheless, the catalyst spheres still possess good recyclability.

Figs. S2 and S3 are the ^{31}PNMR spectra of the model oil before and after the reaction. There were no P peaks in both ^{31}PNMR spectra, indicating that there was no P element in model oil before and after the reaction. Therefore, the active species HPW would not fall off into the reaction system. In addition, Fig. S4 showed that no carbon carriers would exfoliate into model oil after the reaction. Hence, HPW/3D-CSs has good stability in the reaction process.

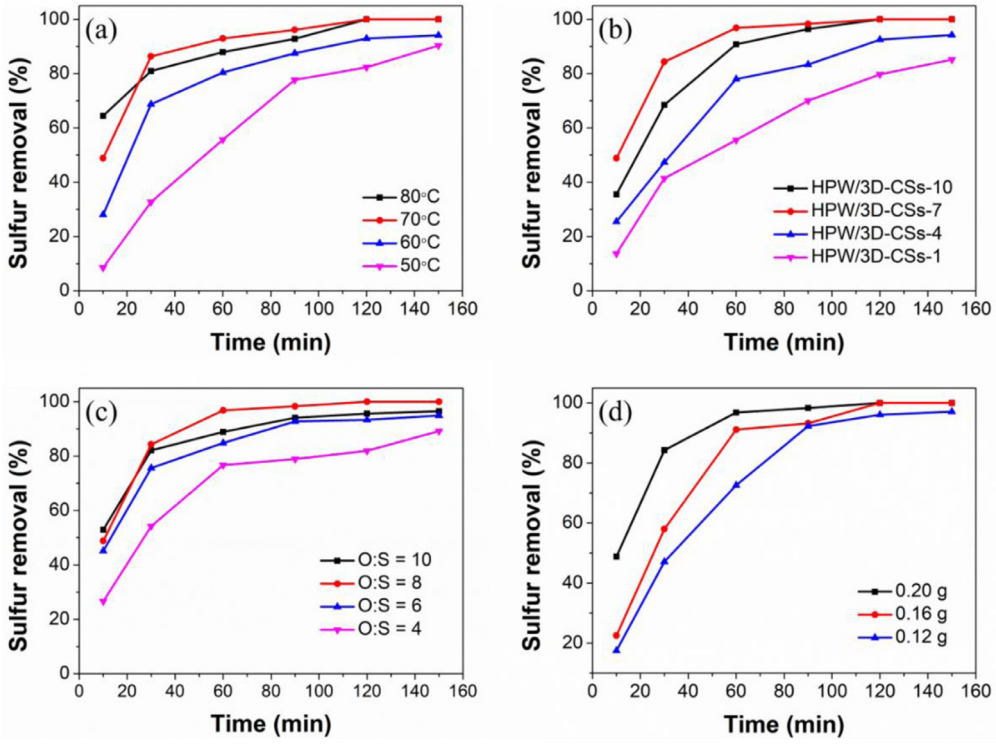

Fig. 4. (a) The effects of different reaction temperatures on desulfurization activity of catalysts, (b) the effects of different loading capacities on desulfurization activity of catalysts, (c) the effects of different oxygen-sulfur ratios on desulfurization activities of catalysts, (d) the effects of the catalyst dosage on desulfurization activity of catalysts. Experimental conditions: *V* (Oil, DBT, 200 ppm of S content) = 5 mL, *V* (HAc) = 1 mL.

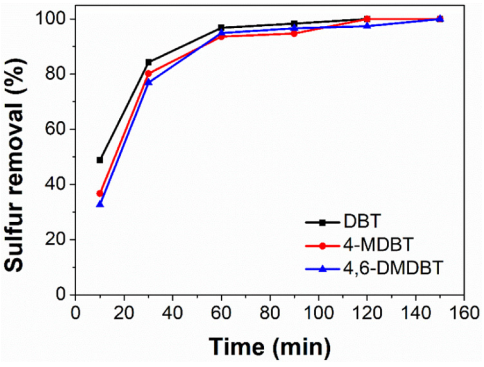

Fig. 5. Removal of different substrates in the desulfurization reaction. Experimental conditions: *V* (Oil, 200 ppm of S content) = 5 mL, *V* (HAc) = 1 mL, *m* (catalyst) = 0.20 g (five HPW/3D-CSs, ± 5%), *T* = 70 °C, *n* (O/S) = 8.

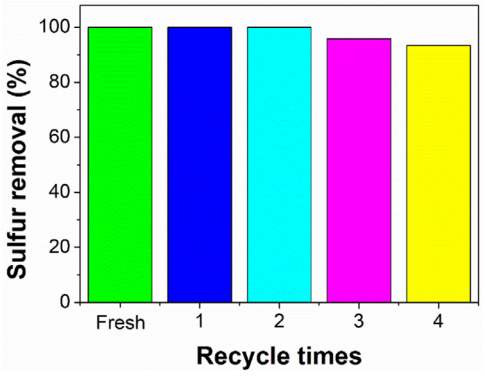

Fig. 7. The recycle performance of the catalyst. Experimental conditions: *V* (Oil, DBT, 200 ppm of S content) = 5 mL, *V* (HAc) = 1 mL, *m* (catalyst) = 0.20 g (five HPW/3D-CSs, ± 5%), *T* = 70 °C, *n* (O/S) = 8.

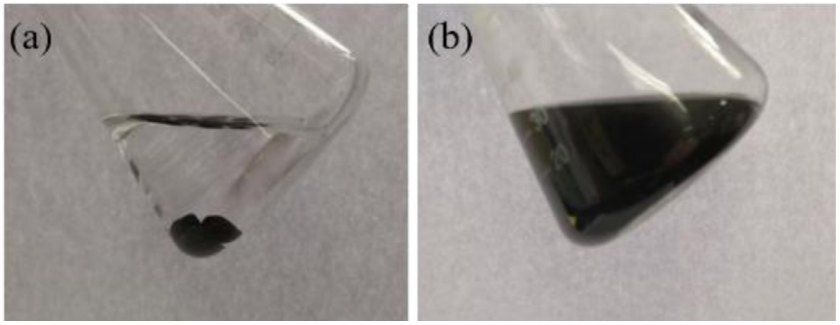

Fig. 6. Photos of different desulfurization systems: (a) 3D-printed catalyst; (b) traditional powder catalyst.

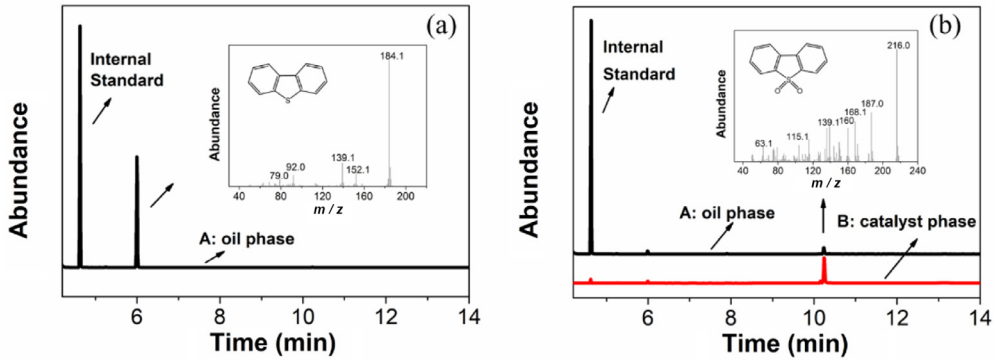

Fig. 8. The GC–MS of main compounds of (a) the unreacted model oil, (b) the reacted oil phase (A) and the catalyst phase (B). Experimental conditions: *V* (Oil, DBT, 200 ppm of S content) = 5 mL, *V* (HAc) = 1 mL, *m* (catalyst) = 0.2 g (five HPW/3D-CSs, ± 5%), *T* = 70 °C, *n* (O/S) = 8.

3.5. Analysis of oxidizing products by GC–MS

For further studying the reaction process of the ODS system, the oxidation products of DBT were detected by gas chromatography-mass spectrometry (GC–MS) [69]. After the reaction, the catalyst phase was separated from the oil phase, and the oil phase was filtered by filter membrane and injected into GC–MS detector to measure the residual sulfide and reaction products. The catalyst phase was extracted by carbon tetrachloride for extraction and analyzed by GC–MS. According to Fig. 8(a), only DBT can be detected in the pristine model oil. Fig. 8(b) indicated that $DBTO_2$ was mainly adsorbed in catalyst phase, and rarely in the oil phase. Compared with Fig. 8(a), $DBTO_2$ was the oxidizing product of DBT after reaction.

Hence, it was inferred that hydrogen peroxide was first adsorbed on the surface of HPW/3D-CSs. HPW can produce corresponding polyperoxide intermediates [70]. At the same time, the model oil was fully contacted with the catalyst in the acetic acid system under intense stirring. DBT was adsorbed on the surface of HPW/3D-CSs through the π–π interaction [71]. Then DBT was oxidized to $DBTO_2$ by the action of polyperoxide intermediates [42]. As shown in the GC–MS results, the only oxidation product $DBTO_2$ was detected in the catalyst phase.

4. Conclusions

In conclusion, a 3D printing method was employed to construct integral spheres with sizes of centimeter-level. The obtained porous structure of the HPW/3D-CSs is beneficial to the mass transfer during the catalytic oxidative desulfurization process, while the integral structure of the HPW/3D-CSs is in favor of the separation of the catalyst from oxidative desulfurization system. The as-prepared HPW/3D-CSs obtained a 100% of sulfur removal from model oil, and the reaction parameters were also optimized. Besides, the easily recycled 3D-printed catalyst can be reused for 5 times without significantly reducing catalytic performance. In addition, the reaction products and the reaction mechanism were deduced by GC–MS analysis. The 3D-printed method would provide a novel strategy for preparation of catalysts with integral structure, which is simple and easy for separation.

Declaration of Competing Interest

None.

Acknowledgments

This work was financially supported by the National Natural Science Foundation of China (Nos. 21722604, 21576122, 21878133), China Postdoctoral Science Foundation (No. 2019M651743).

Supplementary material

Supplementary material associated with this article can be found, in the online version, at doi:10.1016/j.jechem.2019.10.001.

References

[1] F. Lin, D. Wang, Z. Jiang, Y. Ma, J. Li, R. Li, C. Li, Energy Environ. Sci. 5 (2012) 6400–6406.
[2] J. Xu, S. Zhao, W. Chen, M. Wang, Y.F. Song, Chem. Eur. J. 18 (2012) 4775–4781.
[3] W. Li, H. Tang, T. Zhang, Q. Li, J. Xing, H. Liu, AIChE J. 56 (2010) 1391–1396.
[4] J. Yin, J. Wang, Z. Li, D. Li, G. Yang, Y. Cui, A. Wang, C. Li, Green Chem. 17 (2015) 4552–4559.
[5] F.T. Li, B. Wu, R.H. Liu, X.J. Wang, L.J. Chen, D.S. Zhao, Chem. Eng. J. 274 (2015) 192–199.
[6] Y. Nie, C. Li, A. Sun, H. Meng, Z. Wang, Energy Fuels 20 (2006) 2083–2087.
[7] A.E.S. Choi, S. Roces, N. Dugos, M.W. Wan, Fuel 180 (2016) 127–136.
[8] Y. Liu, H. Wang, J. Zhao, Y. Liu, C. Liu, J. Energy Chem. 29 (2019) 8–16.
[9] L. Lin, A. Wang, L. Zhang, M. Dong, Y. Zhang, J. Power Sour. 220 (2012) 138–146.
[10] Y. Chi, C. Li, Q. Jiao, Q. Liu, P. Yan, X. Liu, U. Welz-Biermann, Green Chem. 13 (2011) 1224–1229.
[11] F.J. Méndez, O.E. Franco-López, X. Bokhimi, D.A. Solís-Casados, L. Escobar-Alarcón, T.E. Klimova, Appl. Catal. B: Environ. 219 (2017) 479–491.
[12] H. Song, J. Gao, X. Chen, J. He, C. Li, Appl. Catal. A: Gen. 456 (2013) 67–74.
[13] X. Chen, D. Song, C. Asumana, G. Yu, J. Mol. Catal. A: Chem. 359 (2012) 8–13.
[14] K. Chen, N. Liu, M. Zhang, D. Wang, Appl. Catal. B: Environ. 212 (2017) 32–40.
[15] Z. Li, C. Li, Y. Chi, A. Wang, Z. Zhang, H. Li, Q. Liu, U. Welz-Biermann, Energy Fuels 26 (2012) 3723–3727.
[16] Z. Song, T. Zhou, J. Zhang, H. Cheng, L. Chen, Z. Qi, Chem. Eng. Sci. 129 (2015) 69–77.
[17] C. Li, D. Li, S. Zou, Z. Li, J. Yin, A. Wang, Y. Cui, Z. Yao, Q. Zhao, Green Chem. 15 (2013) 2793–2799.
[18] Z. Li, J. Xu, D. Li, C. Li, RSC Adv. 5 (2015) 15892–15897.
[19] X. Ren, Z. Liu, L. Dong, G. Miao, N. Liao, Z. Li, J. Xiao, AIChE J. 64 (2018) 2146–2159.
[20] Y. Yin, D.M. Xue, X.Q. Liu, G. Xu, P. Ye, M.Y. Wu, L.B. Sun, Chem. Commun. 48 (2012) 9495–9497.
[21] J. Xiao, X. Wang, Y. Chen, M. Fujii, C. Song, Ind. Eng. Chem. Res. 52 (2013) 15746–15755.
[22] D. Fang, Q. Wang, Y. Liu, L. Xia, S. Zang, Energy Fuels 28 (2014) 6677–6682.
[23] W. Ding, W. Zhu, J. Xiong, L. Yang, A. Wei, M. Zhang, H. Li, Chem. Eng. J. 266 (2015) 213–221.
[24] D. Zhao, Z. Sun, F. Li, R. Liu, H. Shan, Energy Fuels 22 (2008) 3065–3069.
[25] S. Gao, X. Chen, R. Abro, A.A. Abdeltawab, S.S. Al-Deyab, G. Yu, Ind. Eng. Chem. Res. 54 (2015) 9421–9430.
[26] P. Wu, Y. Wu, L. Chen, J. He, M. Hua, F. Zhu, X. Chu, J. Xiong, M. He, W. Zhu, H. Li, Chem. Eng. J. 380 (2020) 122526.
[27] S. Gao, X. Chen, X. Xi, M. Abro, W. Afzal, R. Abro, G. Yu, ACS Sustain. Chem. Eng. 7 (2019) 5660–5668.
[28] Q. Gu, Y. Ding, Z. Liu, Y. Lin, R. Schloegl, S. Heumann, D. Su, J. Energy Chem. 32 (2019) 131–137.
[29] A. Liu, M. Zhu, B. Dai, Appl. Catal. A: Gen. 583 (2019) 117134.

[30] S. Pérez-Rodríguez, D. Sebastián, M.J. Lázaro, Electrochim. Acta 303 (2019) 167–175.
[31] B. Jiang, H. Yang, L. Zhang, R. Zhang, Y. Sun, Y. Huang, Chem. Eng. J. 283 (2016) 89–96.
[32] M.H. Ibrahim, M. Hayyan, M.A. Hashim, A. Hayyan, Renew. Sustain. Energy Rev. 76 (2017) 1534–1549.
[33] H. Li, B. Zhang, W. Jiang, W. Zhu, M. Zhang, C. Wang, J. Pang, H. Li, Green Energy Environ. 4 (2019) 38–48.
[34] X. Li, X. Yang, F. Zhou, J. Zhang, H. Yang, Y. Wang, Y. Zhao, X. Yuan, J. Ju, S. Hu, J. Taiwan Inst. Chem. E. 100 (2019) 210–219.
[35] R. Zhao, X. Li, J. Su, X. Gao, Appl. Surf. Sci. 392 (2017) 810–816.
[36] M. Huang, G. Chang, Y. Su, H. Xing, Z. Zhang, Y. Yang, Q. Ren, Z. Bao, B. Chen, Chem. Commun. 51 (2015) 12205–12207.
[37] R. Ghubayra, C. Nuttall, S. Hodgkiss, M. Craven, E.F. Kozhevnikova, I.V. Kozhevnikov, Appl. Catal. B: Environ. 253 (2019) 309–316.
[38] Z.H. Ma, H.B. Han, Z.B. Zhou, J. Nie, J. Mol. Catal. A: Chem. 311 (2009) 46–53.
[39] J. Shangguan, Y. Zhao, H. Fan, L. Liang, F. Shen, M. Miao, Fuel 108 (2013) 80–84.
[40] M.A. Alvarez-Amparán, L. Cedeño-Caero, Catal. Today 282 (2017) 133–139.
[41] X. Yao, C. Wang, H. Liu, H. Li, P. Wu, L. Fan, H. Li, W. Zhu, Ind. Eng. Chem. Res. 58 (2019) 863–871.
[42] A.K. Dizaji, B. Mokhtarani, H.R. Mortaheb, Fuel 236 (2019) 717–729.
[43] J. Xiong, L. Yang, Y. Chao, J. Pang, P. Wu, M. Zhang, W. Zhu, H. Li, Green Chem. 18 (2016) 3040–3047.
[44] H. Ji, J. Sun, P. Wu, Y. Wu, J. He, Y. Chao, W. Zhu, H. Li, Fuel 213 (2018) 12–21.
[45] P. Wu, W. Zhu, Y. Chao, J. Zhang, P. Zhang, H. Zhu, C. Li, Z. Chen, H. Li, S. Dai, Chem. Commun. 52 (2016) 144–147.
[46] H. Lü, W. Ren, H. Wang, Y. Wang, W. Chen, Z. Suo, Appl. Catal. A: Gen. 453 (2013) 376–382.
[47] F. Ye, G. Miao, L. Wu, Y. Wu, Z. Li, C. Song, J. Xiao, Chem. Eng. Sci. 168 (2017) 225–234.
[48] X. Wang, Q. Guo, X. Cai, S. Zhou, B. Kobe, J. Yang, ACS Appl. Mater. Inter. 6 (2014) 2583–2587.
[49] S. Rossi, R. Porta, D. Brenna, A. Puglisi, M. Benaglia, Angew. Chem. Int. Ed. 56 (2017) 4290–4294.
[50] J.C. Ruiz-Morales, A. Tarancón, J. Canales-Vázquez, J. Méndez-Ramos, L. Hernández-Afonso, P. Acosta-Mora, J.R. Marín Rueda, R. Fernández-González, Energy Environ. Sci. 10 (2017) 846–859.
[51] R.D. Farahani, M. Dube, D. Therriault, Adv. Mater. 28 (2016) 5794–5821.
[52] A.J. Capel, R.P. Rimington, M.P. Lewis, S.D.R. Christie, Nat. Rev. Chem. 2 (2018) 422–436.
[53] M.R. Hartings, Z. Ahmed, Nat. Rev. Chem. 3 (2019) 305–314.
[54] X. Zhou, C.J. Liu, Adv. Funct. Mater. 27 (2017) 1701134.
[55] A.S. Diaz-Marta, C.R. Tubio, C. Carbajales, C. Fernandez, L. Escalante, E. Sotelo, F. Guitian, V. Laura Barrio, A. Gil, A. Coelho, ACS Catal. 8 (2018) 392–404.
[56] C. Parra-Cabrera, C. Achille, S. Kuhn, R. Ameloot, Chem. Soc. Rev. 47 (2018) 209–230.
[57] X. Sun, Y. Yan, L. Zhang, G. Ma, Y. Liu, Y. Yu, Q. An, S. Tao, Adv. Mater. Interfaces 5 (2018) 1701626.
[58] E. Fantino, A. Chiappone, I. Roppolo, D. Manfredi, R. Bongiovanni, C.F. Pirri, F. Calignano, Adv. Mater. 28 (2016) 3712–3717.
[59] S.Y. Dou, R. Wang, Chem. Eng. J. 369 (2019) 64–76.
[60] X.M. Yan, P. Mei, J. Lei, Y. Mi, L. Xiong, L. Guo, J. Mol. Catal. A: Chem. 304 (2009) 52–57.
[61] X. Liao, Y. Huang, Y. Zhou, H. Liu, Y. Cai, S. Lu, Y. Yao, Appl. Surf. Sci. 484 (2019) 917–924.
[62] Y. Zhang, R. Wang, Appl. Catal. B: Environ. 234 (2018) 247–259.
[63] A.A. Novikova, V.E. Burlakova, V.N. Varavka, I.E. Uflyand, E.G. Drogan, V.A. Irkha, J. Mol. Liq. 284 (2019) 1–11.
[64] U. Arellano, J.M. Shen, J.A. Wang, M.T. Timko, L.F. Chen, J.T. Vázquez Rodríguez, M. Asomoza, A. Estrella, O.A. González Vargas, M.E. Llanos, Fuel 149 (2015) 15–25.
[65] Y. Qin, S. Xun, L. Zhan, Q. Lu, M. He, W. Jiang, H. Li, M. Zhang, W. Zhu, H. Li, New J. Chem. 41 (2017) 569–578.
[66] S. Xun, W. Zhu, Y. Chang, H. Li, M. Zhang, W. Jiang, D. Zheng, Y. Qin, H. Li, Chem. Eng. J. 288 (2016) 608–617.
[67] S. Otsuki, T. Nonaka, N. Takashima, W.H. Qian, A. Ishihara, T. Imai, T. Kabe, Energy Fuels 14 (2000) 1232–1239.
[68] H.X. Qi, S.R. Zhai, W. Zhang, B. Zhai, Q.D. An, Catal. Commun. 72 (2015) 53–56.
[69] X. Xiao, H. Zhong, C. Zheng, M. Lu, X. Zuo, J. Nan, Chem. Eng. J. 304 (2016) 908–916.
[70] H. Yang, B. Jiang, Y. Sun, L. Zhang, Z. Huang, Z. Sun, N. Yang, J. Hazard. Mater. 333 (2017) 63–72.
[71] A.K. Dizaji, H.R. Mortaheb, B. Mokhtarani, J. Mater. Sci. 51 (2016) 10092–10103.